International Journal of Thermofluids 21 (2024) 100556

Contents lists available at ScienceDirect

International Journal of Thermofluids

journal homepage: www.sciencedirect.com/journal/international-journal-of-thermofluids

Energy, exergy and thermo-economics analyses of hybrid solar, steam turbine and biomass gasification system for hydrogen production by polymer membrane electrolyzer

Kairat Kuterbekov, Asset Kabyshev *, Kenzhebatyr Bekmyrza, Marzhan Kubenova

L.N. Gumilyov Eurasian National University, 010008, Satpayev st. 2, Astana, Kazakhstan

ARTICLE INFO

Keywords:
Exergy
Thermo-economics
Hydrogen
Biomass
Polymer membrane electrolyzer
Hybrid system

ABSTRACT

This study presents an evaluation of the energy exergy and thermo-economics of a hybrid power generation system that simultaneously produces power, heat, and hydrogen using solar and biomass energy. The system employs a polymer membrane electrolyzer for hydrogen production, with heat exchangers utilized to attain the desired water temperature instead of conventional heaters. The steam turbine section is heated using exhaust gas from the combustion chamber and heated water from the condenser. Simulation of the system's thermodynamic, exergy, and exergy-economic analyses was conducted using the ESS tool. Analytical assessments were performed based on the provided data. The system achieves a power output of 25 MW, marking the highest level for solar-based systems. The results showed that the cost of the solar section, which constitutes around 68 % of the overall cost, rises with the number of mirrors. The exergy destruction rate of the entire system decreases from 25.71 MW to 24.95 MW. The total cost of operating the system increases by 175.5 dollars per hour at the highest temperature and decreases by 173 dollars per hour at the lowest temperature. The power consumption of electrolyzers directly affects the overall cost of the system, with a range of 0.05 to 0.07 MW resulting in total cost changes of 1.52 USD per hour. The transition to the work requiring the most energy by the electrolyzer causes a loss of 0.27 MW of exergy.

Introduction

The increase in energy consumption plays a pivotal role in the advancement of human societies, and scientists contemplate the utilization of energy resources [1–3]. This issue poses a threat to a variety of issues, including environmental concerns, water conflicts, and even the survival of humans [4,5]. In point of fact, one of the problems that arises as a consequence of an excessive reliance on non-renewable fuels and resources is the escalation of severe environmental conditions that were already present, such as urban flooding, drought, and climate change [6,7]. In contemporary industrial societies, in addition to the peril of the swift exhaustion of fossil resources, the emissions stemming from these resources have resulted in irreversible repercussions for the planet [8–10]. Energy consumption is projected to rise in recent future [11]. The primary factors contributing to this phenomenon are the global population growth, the aspiration for greater societal well-being, and the rise in per capita gross domestic product worldwide [12]. This process presents a misleading portrayal of the world in the near future, compelling humans to seek a resolution for this predicament. Research indicates that there are two primary approaches to address this issue: enhancing energy efficiency and augmenting the proportion of clean and sustainable energy sources in the global energy, where renewable energies derived from natural sources are included, wind, tides, waves, sun, and biomass [13,14]. Nowadays, biomass and solar energy have garnered significant interest from researchers due to their environmental benefits [15]. Some of the benefits include ample resources, enhanced safety, decreased greenhouse gas emissions, and contributing to global warming [16,17].

Biomass is a carbon-based mixture consisting of organic molecules, which contain hydrogen, oxygen, nitrogen, as well as trace amounts of alkalis and heavy metals [18]. As biomass grows, it sequesters carbon dioxide from the surroundings and stores it as carbon. However, when biomass is burned, it releases the stored carbon dioxide back into the environment. In contrast, the combustion of fossil fuels contributes to environmental pollution [19,20]. Gasification is a method of utilizing biomass energy by converting it into flammable gases [21]. Hydrogen energy, being an environmentally friendly fuel, is the foremost

* Corresponding author.
E-mail address: assetenu@gmail.com (A. Kabyshev).

https://doi.org/10.1016/j.ijft.2023.100556

Available online 28 December 2023

Nomenclature

H	Enthalpy
S	Entropy
T	Temperature of the electrolyzer (°C)
R	Universal constant of gases
n	Number of electrons that have been traded
F	Faraday constant
P_{H2}	Pressure of hydrogen (Pa)
P_{O2}	Pressure of oxygen (Pa)
P_{H2O}	Pressure of water (Pa)
V_{act}	Activation voltage drop (v)
V_{ohm}	Ohmic voltage drop (v)
$J_{0,i}$	Anode/Cathode current exchange density (A/cm^2)
J_i^{ref}	Anode/Cathode reference current exchange density (A/cm^2)
$E_{act,i}$	Activation energy (kJ/mol)
LHV	Low heating value of hydrogen
$\dot{N}_{H_2,\text{out}}$	Hydrogen output from the electrolyzer
W_{elec}	Energy input to the electrolyzer
$Ex_{\text{heat,pem}}$	Thermal energy input rate to the electrolyzer (kJ/mol)
K_1 and K_2	Equilibrium constants (Associated with the Gibbs function)
ΔG_1^0 and ΔG_2^0	Gibbs function variation

alternative for substituting fossil fuels worldwide in the future [22,23]. Numerous developed nations have made significant strides towards utilizing this energy, and there is a rapid push to globalize and commercialize it. Nevertheless, hydrogen is not naturally occurring in isolation and lacks the inherent capability for direct production [24]. Additionally, a substantial amount of energy is required to separate it. Given that the primary energy source for hydrogen production still relies on fossil fuels, it is imperative to shift towards non-fossil fuel sources and leverage the potential of renewable energy sources for hydrogen production [25].

Hydrogen, the most prevalent element in the universe, is widely anticipated to serve as humanity's primary fuel source in the future [26,27]. Hydrogen, similar to fossil fuels and natural gas, is not easily accessible in its natural state [28]. Consequently, its production necessitates financial investment and the utilization of primary energy, which should be obtained plentifully and at a competitive cost from specific sources [29]. Hydrogen gas undergoes combustion with optimal efficiency, resulting in a relatively thorough completion of the combustion reaction. The application of hydrogen as an energy source is highly significant due to its crucial economic and environmental implications [30]. The water electrolysis method, which follows the natural gas reforming method, is widely recognized as one of the most prominent techniques for producing hydrogen from non-fossil sources [31]. Generating hydrogen on a large scale necessitates a substantial input of energy, either in the form of electricity or heat. The electrolysis of water has been employed as one of the earliest techniques for hydrogen production [32]. Electrolysis is the procedure by which water is decomposed, necessitating the application of heat and electricity to isolate hydrogen and oxygen from one another. Typically, hydrogen, due to its value, is stored in reservoirs for future utilization [33].

Recently, researchers have prioritized discovering novel methods for energy provision that emphasize the efficient utilization of current resources and safeguarding the environment [34–37]. Bai et al. [38] presented and investigated a new hybrid power generation system aimed at maximizing the use of renewable energies. By receiving and concentrating solar radiation, those flat collectors raise the temperature of the heat transfer fluid (synthetic oil) to 319 °C, where it becomes steam as it passes through the heat exchangers. It is manufactured at a temperature of 371 °C. Solar energy now has a net annual return on investment of 13.18 %. Furthermore, biomass consumption has increased by 53.22 % when compared to the normal biomass power generation cycle. Taner et al. [39] developed a system that utilizes advanced technology to generate energy from hydrogen. Additionally, they produced hydrogen gas energy through the process of electrolytic chemical reaction. Moreover, to optimize the performance and efficiency of the electrolysis cells, exceptionally powerful magnets were attached to their external surfaces. The hydrogen gas production was found to be six m^3 per hour. Tukenmez et al. [40] carried out an examination of a facility that utilizes solar and biomass power sources to generate ammonia and hydrogen over the course of several generations. The process of integration has yielded numerous valuable commodities, including hydrogen and electricity. It was determined that the total electrical energy output of the plant was 20.125 kW, with respective energy and exergetic efficiencies of 58.76 % and 55.64 %. Burulday et al. [41] investigated the integration of a biomass-based hydrogen generation system with a solar energy power facility in their study. The primary objective of the proposed facility is to supply the energy required for both the hydrogen synthesis procedure and the generation of electrical power. The power generation systems and the hydrogen production procedure each have exergy efficiencies of 39.6 % and 55.8 %, respectively. The net power generation of the system is ascertained to be 38.89 MW. Shamsi et al. [42] developed a method for producing hydrogen from tars produced during the gasification of lignocellulosic biomass. To maximize the production of hydrogen and enhance energy efficiency. According to the results, the process of producing hydrogen from integrated biomass gasification tars is carbon neutral. Wang et al. [43] developed a multi-criteria evaluation method for an innovative biomass fuel and solid oxide fuel cell-based multigeneration cycle. The outcomes indicate that the proposed multigeneration cycle has the capability to compete effectively with the preponderance of biomass-powered systems. Furthermore, significant reductions in carbon dioxide emissions are achievable when compared to conventional power plants that rely on fossil fuel.

From a thermodynamic perspective, this study evaluated the energy-economic exergy of a system that simultaneously produced hydrogen, electricity, and heat using solar and biomass energy. Hydrogen is generated within this system by means of a polymer membrane electrolyzer. Heat exchangers were employed in lieu of heaters in order to attain the intended water temperature. The steam turbine component is heated by utilizing exhaust gas from the combustion chamber and heated water from the condenser. The ESS tool was utilized to simulate the thermodynamic, exergy, and exergy-economic analyses of the investigated system.

Materials and methods

The electrolysis of water is generally regarded as being among the most important processes that can be carried out, right after the method of reforming natural gas, which is one of the most important processes that can be carried out. It is necessary to make use of either thermal energy or electrical energy in order to convert hydrogen into significant quantities of energy during the process of mass production. This is the case regardless of whether the energy in question is thermal or electrical. The process of electrolysis involves the use of an electric current in conjunction with heat energy to separate water into its component parts, hydrogen and oxygen, respectively. This is accomplished by breaking the water molecule down using an electric current. The investigation into the process that is responsible for the production of hydrogen is made easier by the utilization of a system that is comprised of polymer membrane electrolyzers. In a polymer membrane electrolyzer, water molecules and protons must travel across the electrolyzer's membrane in order to get from the anode to the cathode. When the membrane reaches the anode of the battery, it deteriorates into oxygen, protons, and

electrons. In order to help facilitate the release of electrons from the cell, an external circuit is used. A combination reaction involving protons and electrons takes place at the cathode in order to produce hydrogen gas. This reaction is the result of the production of hydrogen gas. As can be seen in Eq. (1), the polymer membrane electrolyzer's cathode and anode are the locations in which the subsequent reactions take place [44].

$$\begin{aligned} &H_2O \rightarrow 2H^+ + \frac{1}{2}O_2 + 2e^- \text{ Andes} \\ &2H^+ + 2e^- \rightarrow H_2 \text{ ; Cathode} \\ &H_2O_{(l)} \rightarrow H_{2(g)} + \frac{1}{2}O_2(g) \text{ Overall} \end{aligned} \quad (1)$$

The cycle has undergone thermodynamic analysis using EES software. The approach considers the following assumptions.

- The varying in potential and kinetic energy have been disregarded.
- The system operates in a consistent and steady manner.
- Only the chemical exergy of the polymer membrane electrolyzer is taken into account.

System description

The intended cycle is made up of three distinct parts that all work together. The first step is gasification, followed by the use of solar energy, and finally by the use of a steam turbine. In the first stage of the process, biomass is used as a renewable energy source. After being introduced into the combustion chamber, the biomass gasification process serves as a fuel that is burned. The spent fuel from the combustion chamber is fed into the high-pressure turbine to generate power. During the second phase of the cycle, solar energy is used to heat the exhaust gas produced by the high pressure turbine. The combustion gas is routed to the low pressure turbine after it has been heated to produce energy and passed through the first turbine. Furthermore, the turbine exhaust gas is used to pre-heat the water before it enters the electrolyzer. The electrolyzer is in charge of converting water into hydrogen, which is then used by the steam turbine to generate power (Fig. 1).

Polymer membrane electrolyzer

The electrolyzer exhibited exceptional energy efficiency by converting electrical energy into chemical energy, which is then stored in the form of hydrogen [45]. The utilization of polymer membrane technology enabled the effective exchange of protons, thereby enabling the separation of hydrogen and oxygen gases. The electrolyzer's low operating temperatures minimized energy losses and enhanced overall system efficiency [46]. The exergy analysis indicated that the polymer membrane electrolyzer played a substantial role in the exergy flow within the system. The electrolyzer produced a significant amount of hydrogen gas as a result of receiving a high-quality energy input, which contributed to a substantial exergy output [47]. This demonstrates the efficiency of the electrolyzer in harnessing energy for practical purposes.

The electrolyzer's ability to operate at low temperatures and convert energy efficiently makes it a financially advantageous component in the hybrid system [48]. The analysis took into account the expenses related to electricity, maintenance, and other operational costs associated with the electrolyzer. The polymer membrane electrolyzer showed encouraging results in the hybrid system for generating hydrogen. Due to its high energy efficiency, efficient proton exchange, and economic viability, it is a suitable option for sustainable hydrogen generation. Additional research and optimization endeavors can improve the efficiency and economic feasibility of this technology [49–51].

Table 1 lists the fixed parameters that were employed during the modeling process of polymer membrane electrolyzers [52]. Utilizing the Gibbs free energy of the reaction, it is possible to calculate the reversible voltage of the electrolyzer. The voltage that is specified is indicative of the theoretical electrolyzer cell functioning under conditions of reversibility and isothermality. Fuel cells generate electrical energy through the efficient movement of electrons, which is conveniently accessible through an external circuit . The electrolyzer operates on the principle of minimizing energy loss while maximizing the utilization of the generated motive power for hydrogen production. The reversible voltage is supplemented with the residual voltage decreases. An examination of

Table 1
Parameters for polymer membrane electrolyzer modeling.

Parameter	Value
P_{H2}, P_{O2}, P_{H2O}	1 bar
T	253 K
L	180 μm
$E_{act,a}$	75.2 kJ/mol
$E_{act,c}$	18.5 kJ/mol
LHV	225 kJ/mol

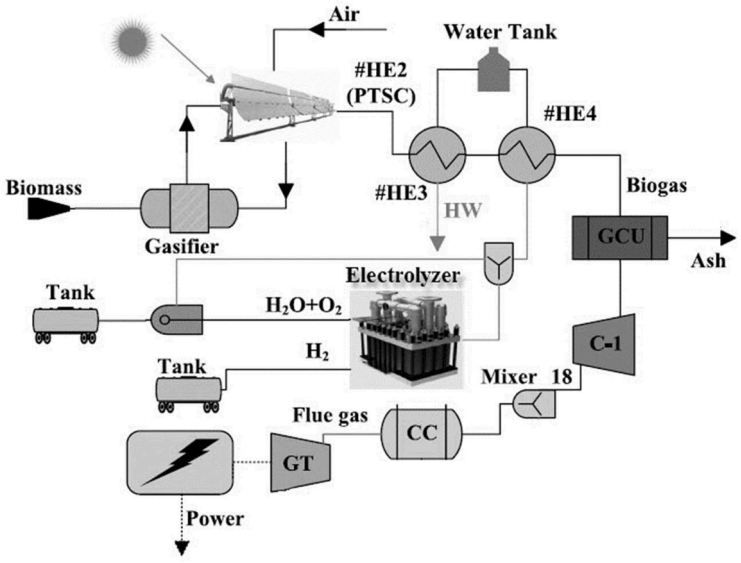

Fig. 1. Hybrid system scheme.

the impact of concentration is conducted with respect to both the equation and concentration reductions. Nevertheless, this article exclusively examines ohmic and activation dips, excluding any discussion of concentration drops. The Gibbs free energy of a reaction is denoted as Eq. (2):

$$\Delta G = \Delta H - \mathrm{T}\Delta S \tag{2}$$

ΔH is the enthalpy variation and $\Delta S$is the entropy variation. Under ideal circumstances, the thermal energy produced by the reaction is consistently extracted from the system, resulting in a constant temperature of the system. The energy released is directly proportional to the product of the entropy changes of the reaction occurring at the fuel cell's operating temperature. Eq. (3) calculates the reversible potential [53]. Using the Nernst equation (Eq. (4)), one can calculate the open circuit voltage of the polymer membrane electrolyzer [54].

$$V_0 = -\frac{\Delta G}{2F} \tag{3}$$

$$V_0 = 1.229 - 0.9 * 10^{-3}(\mathrm{T} - 298) + \frac{RT}{nF}\ln\left(\frac{P_{H_2}P_{O_2}^{0.5}}{P_{H_2O}}\right), \tag{4}$$

where, T denotes the temperature of the electrolyzer, R denotes the universal constant of gases, n denotes the number of electrons that have been traded, F denotes the Faraday constant, P_{H2} denotes the pressure of hydrogen, P_{O2} denotes the pressure of oxygen, and P_{H2O} denotes the pressure of water in terms of its electrical charge. The equation for determining the voltage of the electrolyzer is given in Eq. (5).

$$V = V_0 + V_{\mathrm{act}} + V_{\mathrm{ohm}}, \tag{5}$$

where, V_{act} is the activation voltage drop in the anode and cathode and V_{ohm} is the ohmic voltage drop.

Activation voltage losses

The reduction in activation voltage demonstrates that the electrons are now prepared to participate in the electrochemical reaction that is currently taking place. Because electrons are transferred from the electrode surfaces during the chemical reaction, some of the voltage that is supplied to the electrolyzer is lost (Eq. (8)). In order to make an estimate of the activation energy on both the cathode and the anode sides, the Butler-Volmer equation (Eq. (7)) is applied as a result of the activation voltage drop that occurs.

$$V_{act,i} = \frac{RT}{F}\sinh^{-1}\left(\frac{J}{2J_{0,i}}\right) \tag{6}$$

$$J_{0,i} = J_i^{ref}\mathrm{EXP}\left(\frac{-E_{act,i}}{RT}\right)\ i = a, c. \tag{7}$$

where $J_{0,i}$represents the anode/cathode current exchange density in A/cm^2, J_i^{ref}represents the anode/cathode reference current exchange density in A/cm^2, and $E_{act,i}$ represents the activation energy in *kJ/mol.* The amount of exchange density is affected by a variety of factors, including the type of material and porosity of the electrodes, the concentration, size, and distribution of catalyst particles on the electrodes, as well as the temperature at which the device is being operated. The anode current exchange density for electrodes containing a platinum catalyst falls somewhere in the range of 10^{-5} to 10^{-8} A/m^2, while the cathode current exchange density falls somewhere in the range of 10^{-1} to 10 A/m^2 [55]. In this study, the anode current exchange density is 10^{-3} A/m^2 and the cathode current exchange density is 10 A/m^2 [56].

Ohmic voltage losses

The ohmic voltage drop is the result of the resistance that is created against the flow of electrons as well as the electrical resistance of the polymer membrane electrolyzer. The kind of polymer membrane electrolyzer and electrodes being used will determine the magnitude of this voltage drop. A linear relationship exists between ohmic voltage drop and current density. The resistance of the electrolyzer against the transfer of protons is denoted by "*L*" in Eq. (8), and the ohmic voltage drop that is caused by membrane resistance. The ionic conductivity of the ion exchange membrane (σ_{mem}) in $1/\Omega.cm$ and current density (in terms of A/cm^2) are defined as Eq. (9) [57].

$$V_{ohm} = \frac{L}{\sigma_{mem}}J \tag{8}$$

$$\sigma_{mem} = (0.005139\lambda - 0.00326)\mathrm{EXP}\left[1263\left(\frac{1}{303} - \frac{1}{\tau}\right)\right]. \tag{9}$$

Because water molecules are used to transfer protons across the membrane's surface, the water content (λ) has a significant impact on the ionic conductivity of the membrane. The determination of λ is essential in fuel cells due to the fluctuating humidity of the membrane; however, in polymer membrane electrolyzers, the entire membrane can be considered wet due to the abundance of water on the anode side (also on the cathode side due to the transfer phenomenon). λ typically falls between 14 and 21 [55]. The total energy required is the theoretical energy required to electrolyze water without losses. Real systems, however, experience some loss, and system performance is defined by energy and exergy efficiency (Eqs. (10) and 11).

$$\eta_{\mathrm{pem}} = \frac{\dot{N}_{H_2,\mathrm{out}} \cdot LHV_{H_2}}{W_{\mathrm{elec}} + Q_{\mathrm{heat},pem}} \tag{10}$$

$$\psi_{\mathrm{pem}} = \frac{\dot{N}_{H_2,out} \cdot Ex_{H_2}}{W_{\mathrm{elec}} + Ex_{\mathrm{heat,pem}}}, \tag{11}$$

LHV is the low heating value of hydrogen, $\dot{N}_{H_2,\mathrm{out}}$ is the amount of hydrogen output from the electrolyzer, W_{elec} is the amount of energy input to the electrolyzer, and $Ex_{\mathrm{heat,pem}}$ is the rate of thermal energy input to the electrolyzer. Eqs. (12) to 14 are used to calculate the amount of hydrogen, oxygen, and water output from the electrolyzer.

$$\dot{N}_{H_2,\mathrm{out}} = \frac{J}{2F} = \dot{N}_{H_2\mathrm{o,reacted}} \tag{12}$$

$$N_{O_2,\mathrm{out}} = \frac{J}{4F} \tag{13}$$

$$\dot{N}_{H_2\mathrm{O,out}} = \dot{N}_{\mathrm{H_2O,in}} - \dot{N}_{\mathrm{H_2O,reacted}} = \dot{N}_{H_2\mathrm{O,in}} - \frac{\mathrm{J}}{2\mathrm{F}} \tag{14}$$

$$W_{\mathrm{elec}} = JV. \tag{15}$$

The water flow rate entering the electrolyzer is assumed to be 0.005 *kg/s*. Exergy of hydrogen is defined as Eq. (16):

$$Ex_{H_2} = Ex_{H_2}^{ph} + Ex_{H_2}^{ch}. \tag{16}$$

Both the chemical and the physical exergies of hydrogen are equal to 236 *kJ/kmol* [58], with $Ex_{H_2}^{ph}$ representing the chemical exergy of hydrogen and $Ex_{H_2}^{ch}$ representing the physical exergy of hydrogen. Irreversibility in the polymer membrane electrolyzer as a consequence of heat brought about by the generation of entropy. The entropy production is represented by the Eq. (17) [52].

$$\sigma = 2F\left(V_{act,a} + V_{act,c} + V_{ohm}\right). \tag{17}$$

If $\sigma \geq T\Delta S$ is either equal to or greater than the heat required for decomposition, and the polymer membrane electrolyzer does not require any additional heat from the outside, $Q_{\mathrm{heat,em}} = Ex_{\mathrm{heat,pem}} = 0$. It should be noted that the excess heat produced by it is assumed to be released into the environment via radiation. If $\sigma < T\Delta S$, the heat

produced is less than the heat required, requiring additional heat. Eqs. (18) and 19 are used to calculate the electrolyzer's inlet heat.

$$Q_{\text{heat,pem}} = [T\Delta S - \sigma]N_{\text{H}_2\text{ O, reacted}} = [T\Delta S - \sigma]\frac{\text{J}}{2F} \tag{18}$$

$$Ex_{\text{heat,pem}} = Q_{\text{heat,pem}}\left(1 - \frac{T_0}{T}\right). \tag{19}$$

Biomass gasification modeling

During the initial stages of the modeling process, an examination is conducted on the biomass fuel source by considering the mass components of carbon, hydrogen, oxygen, nitrogen, and sulfur. Additionally, the moisture content in terms of mass percentage, the structural composition of the fuel, and the molar moisture content are determined. The molar amount of gasifying agent is determined by comparing the ratio of fuel to gasifying agent, and the total enthalpy of the reactants is computed. By employing Gibbs free energy minimization and determining the equilibrium constants of the gas composition generated during the gasification process, an estimation can be made in the subsequent stage. The Newton-Raphson method is employed to iteratively refine the results. By equating the enthalpy of the gases produced during gasification with the enthalpy of the biomass fuel and moisture, and considering the reaction temperature, the composition of the resulting gases can be determined. The computed temperature serves as an essential input for the subsequent step of approximating the composition of the resultant gases, and this progression persists until the conditions of thermodynamic and chemical equilibrium are attained. The determination of the final composition of the resulting gases and the corresponding temperature of the reaction allows for the determination of the calorific value of the resulting gases and the efficiency of the process. Gasification will be quantifiable. Fig. 2 illustrates the configuration of a biomass gasification model that relies on a balance-based approach.

The gasification process is an intricate process comprising of numerous chemical reactions that have been characterized by two overarching methods: thermodynamic equilibrium and reaction rate modeling. While the modeling method utilizing reaction rates offers valuable insights into reaction rates and mechanisms, its reliance on numerous parameters hinders its application in power system simulations, which are essential for understanding these systems. It restricts the movement of the hand. Conversely, there exists a thermodynamic equilibrium that is not influenced by the specific configuration of the reactor. During thermodynamic equilibrium, the system reaches its most stable state, characterized by maximum entropy or minimum Gibbs free energy. This study employs the equilibrium thermodynamic method to simulate the gasification process, focusing only on the reactions that involve substantial quantities of gaseous components. Research has demonstrated that all constituents of biogas generated are in the gaseous state. Biogas primarily consists of chemical components with lower molecular weight, notably carbon monoxide, carbon dioxide, water vapor, hydrogen, nitrogen, and methane [59]. For biomass fuel, the gasification reaction with steam is as Eq. (20) [60].

$$CH_aO_b + wH_2O + m(H_2O) \rightarrow n_{H_2H_2} + n_{CO}CO + n_{CO2}CO_2 + n_{H2O}H_2O + n_{CH4}CH_4 + n_C C_{(s)}. \tag{20}$$

The biomass chemical formula is CH_aO_b, where a represents the number of moles of hydrogen (H) and b represents the number of moles of oxygen (O) obtained from the final analysis of biomass. In this context, w represents the moisture content of biomass, while m represents the ratio of kilomoles of steam to kilomoles of biomass, which can also be expressed as the molar ratio of steam to biomass. This variable, which represents the mass ratio of steam to biomass (STBM), is defined as Eq. (21) [60].

$$\text{STBM} = \frac{M_{H2O} \times m}{(M_{\text{biomass}} + M_{H2O} \times w)} \tag{21}$$

The coefficients n_{H2} to n_C are determined by applying the molar balance for carbon (C), hydrogen (H), and oxygen (O). Eqs. (22) and 23 undergo reactions during the gasification process, in the presence of steam [60].

$$CH_4 + H_2O \leftrightarrow CO + 3H_2; \tag{22}$$

$$CO + H_2O \leftrightarrow CO_2 + H_2. \tag{23}$$

The moisture content per mole of biomass is defined as Eq. (24).

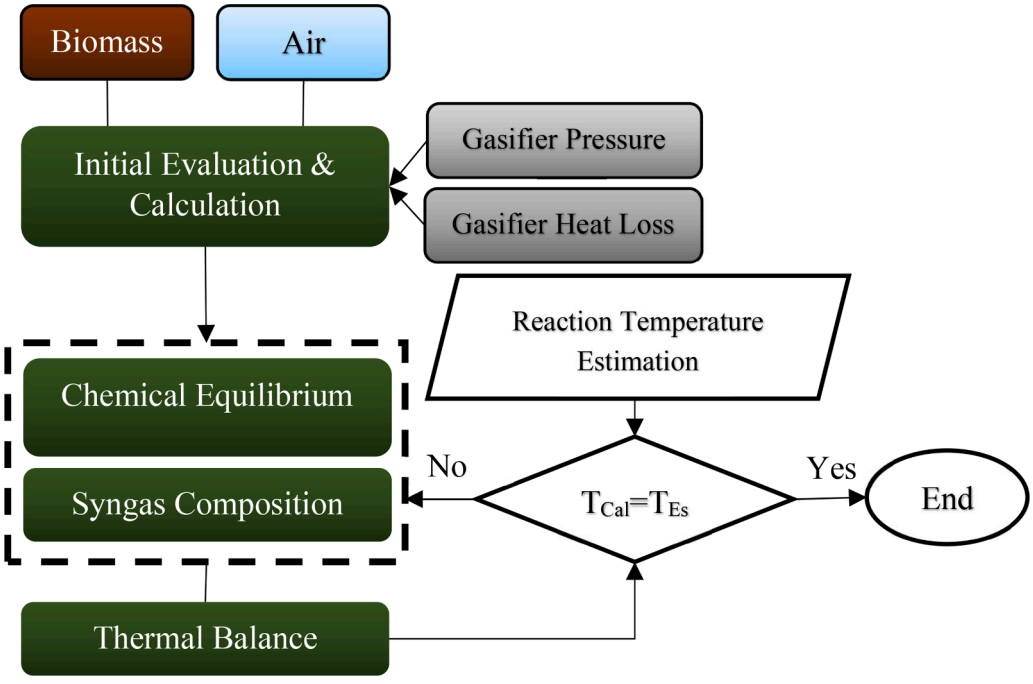

Fig. 2. Gasification thermodynamic analyses process flowchart.

$$W = \frac{M_{biomass} \times MC}{M_{H2O} \times (1 - MC)}. \quad (24)$$

The molecular weights of water and biofuel are denoted as $M_{biomass}$ and M_{H2O}, respectively. MC indicates the moisture content as well. Eqs. (25) and 26 represents the equilibrium constants for the methane decomposition reaction (Eq. (22)) and the gas-water transformation reaction (Eq. (23)) [60].

$$K_1 = \frac{n_{CO} n_{H2}^3}{n_{CH4} n_{H2O}} \left(\frac{P/P_{ref}}{n_{tot}}\right)^2 \quad (25)$$

$$K_2 = \frac{n_{H2} n_{CO2}}{n_{CO} n_{H2O}} \left(\frac{P/P_{ref}}{n_{tot}}\right)^0. \quad (26)$$

where, equilibrium constants K_1 and K_2 are associated with the variations of the Gibbs function in the Eqs. (27) and 28 [60].

$$-\frac{\Delta G_1^0}{\overline{R}T} = \ln K_1 \quad (27)$$

$$-\frac{\Delta G_2^0}{\overline{R}Tg} = \ln K_2. \quad (28)$$

The variables ΔG_1^0 and ΔG_2^0 represent the respective changes in the free Gibbs function of the gas-water transformation reaction and the methane decomposition equation. Under the assumption of adiabatic gasification at the specified temperature, the following energy balance equation (Eq. (29)) can be solved in order to determine the molar ratio of biomass to steam:

$$\begin{aligned} &\bar{h}_{f-\ biomass}^0 + w \times \left(\bar{h}_{f-H2O}^0 + H_{vap}\right) + m \times \left(\bar{h}_{f-\ steam}^0\right) \\ &= n_{H2}\left(\bar{h}_{f-H2}^0 + \Delta\bar{h}_{H2}\right) + n_{CO}\left(\bar{h}_{f-CO}^0 + \Delta\bar{h}_{CO}\right) + n_{CO2}\left(\bar{h}_{f-CO2}^0 + \Delta\bar{h}_{CO2}\right) \\ &+ n_{H2O}\left(\bar{h}_{f-H2O}^0 + \Delta\bar{h}_{H2O}\right) + n_{CH4}\left(\bar{h}_{f-CH4}^0 + \Delta\bar{h}_{CH4}\right) + n \\ &\times n_C\left(\bar{h}_{f-C(s)}^0 + \Delta\bar{h}_{C(s)}\right). \end{aligned} \quad (29)$$

The data required for modeling the biomass gasification process in the hybrid system with steam are presented in Table 2.

Economic analysis

As a powerful tool for the systematic study and optimization of energy systems, this type of analysis combines exergy analysis and cost calculation. Having knowledge of the exergy cost associated with the part allows for a comprehensive analysis of the part's economic viability, taking into account factors such as design, repair and maintenance, and investment costs. Economic exergy analysis is a useful tool for determining the relationship between input costs such as fuel and investment costs, and production costs. The exergy cost for a system component with input current (i) and output current (e) is as Eq. (30).

$$\dot{C} = c\dot{E}x, \quad (30)$$

where, c is the cost in the exergy unit in $GJ/\$$, and $\dot{E}x$ is the exergy rate. Eq. (31) defines the cost balance of the system for each component of the system.

Table 2
Input data to the gasification reactor.

Parameter	Value
Inlet steam temperature	500 °C
Biomass temperature	24 °C
Outlet gas temperature	800 °C
Pressure	1 bar

$$\sum \dot{C}_{out,k} + \dot{C}_{w,k} = \sum \dot{C}_{in,k} + \dot{C}_{q,k} + \dot{Z}_{k,PY}, \quad (31)$$

where,

$$\dot{Z}_{k,PY} = Z_k^0 \cdot \frac{CI_{k,PY}}{CI^0}. \quad (32)$$

In this regard, the total value of the outflows equals the total cost of inputs plus investment, maintenance, and other expenses. According to Eqs. (33) and 34, the total costs associated with the initial investment $Z_k^{0,CI}$ and maintenance costs $Z_k^{0,OM}$ are defined as a single parameter called $\dot{Z}_k^0$.

$$\dot{Z}_k^0 = Z_k^{0,CI} + Z_k^{0,OM}, \quad (33)$$

$$\dot{Z}_k^0 = \frac{z_k \cdot CRF \cdot \varphi}{N}. \quad (34)$$

z_k is the initial purchase price of the device *k-th* (calculated based on thermodynamic parameters), φ is the repair and maintenance coefficient, N is the annual operating hours at full load, and CRF is the cold return coefficient (Eq. (35)). The rate determines the rate of return on capital. The interest (i_r) and the number of years of operation of the devices (n) are calculated according to the values of these two parameters. Accordingly, the interest rate is considered to be between 0.10 and 0.12.

$$CRF = \frac{i_r(1+i_r)^n}{(1+i_r)^n - 1}. \quad (35)$$

The cost equations used in the economic assessments for system components are given in Table 3 [61].

Fig. 3a shows that the solar sector has the highest cost. Fig. 3b shows that the solar component accounts for approximately 67 % of the total cost.

System overall efficiency

Calculating the energy and exergy efficiency of each individual component of the solar hydrogen production system (Eq. (36) and 37) results in the determination of the overall energy and exergy efficiency of the system.

$$\eta_{energy} = \eta_{solar} * \eta_{RE} * \eta_{GEN} * \eta_{pem} \quad (36)$$

$$\psi_{energy} = \psi_{solar} * \psi_{RE} * \psi_{GEN} * \psi_{pem}. \quad (37)$$

Exergy destruction

As a necessary part of the second law analysis, the evaluation of exergy destruction or irreversibility in system components is important for finding out how much each component contributes to the overall exergy destruction. The majority of the exergy lost in the gasifier is the result of chemical reactions. It is the solar component that experiences the greatest exergy loss among all the elements comprising the heliostat

Table 3
System components cost equations.

Component	Equation
Gasification reactor	$Z_{gasifier} = 1600 \times \left(\dot{m}_{drybiomass}\left[\frac{kg}{h}\right]\right)^{0.67}$
Afterburner chamber	$Z_{AB} = \left(\frac{46.08 \times \dot{m}_{17}}{(0.955 - (P_{13}/P_4)}\right) \times (1 + e^{0.018T_{13} - 26.4})$
Air compressor	$Z_{AC} = 916 \times (\dot{W}_{AC}/455)^{0.67}$
Fuel compressor	$Z_{FC} = 916 \times (\dot{W}_{FC}/455)^{0.67}$
Air heat exchanger	$Z_{AHX} = 390 \times (A_{AHX}/0.093)^{0.78}$
Fuel heat exchanger	$Z_{FHX} = 130 \times (A_{FHX}/0.093)^{0.78}$
AC-DC Inverter	Z_{inv}=100000×

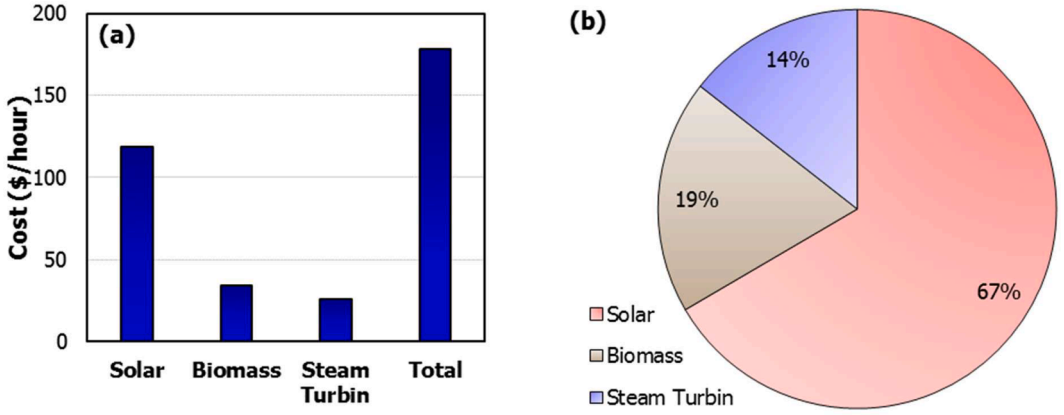

Fig. 3. a) The cost and b) percentage cost of the system main components.

mirror system. The amount of exergy lost by each section is illustrated in Fig. 4a. The solar industry is characterized by the highest exergy destruction percentage. The exergy destruction is attributed to the solar component of the system, which accounts for 50 % of the total exergy destruction. The percentage of exergy destruction in each component of the system is illustrated in Fig. 4b.

Results and discussion

The results presented in this section outline the findings obtained from a comprehensive investigation. It is aimed at providing a succinct yet comprehensive overview of the outcomes derived from the conducted experiments and analyses. The following outcomes shed light on the crucial insights garnered through meticulous data collection and rigorous statistical scrutiny, further contributing to the advancement of our understanding in the field.

Model validation

Electrolyzer model

To ascertain the validity of the electrolyzer model examined in this article, experimental results [62] were compared with the outcomes presented in this article. Nafion is the electrolyte utilized in the experiment. The electrode material employed on the cathode side is platinum. The electrolyzer's polarization diagram is illustrated in Fig. 5. The thickness of the electrolyzer membrane was 50 μm in this assessment. The results of the modeling are in excellent agreement with the experimental data (The root mean square error is 0.08 v).

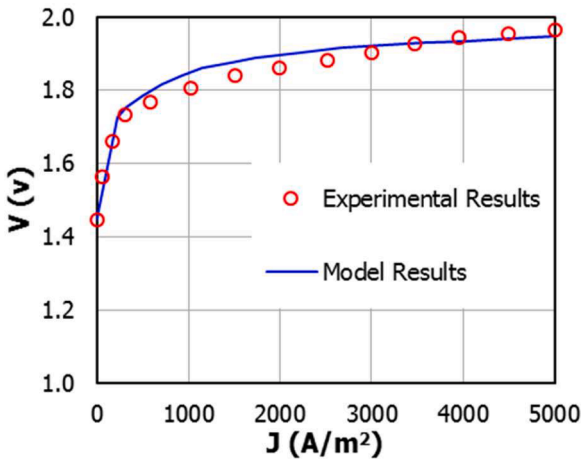

Fig. 5. Comparison of experimental data and numerical modeling results for electrolyzer model.

Biomass gasification model

To verify the accuracy of the gasification model, a comparison was made between the percentage of gas components produced through gasification using steam agents and the findings reported in reference [63]. The strong concurrence among the values presented in Table 4 validates the accuracy of the current model (RMSE = 0.1).

Following that, the total energy yield, total exergy yield, total exergy destruction, and total cost of the system will be calculated by examining

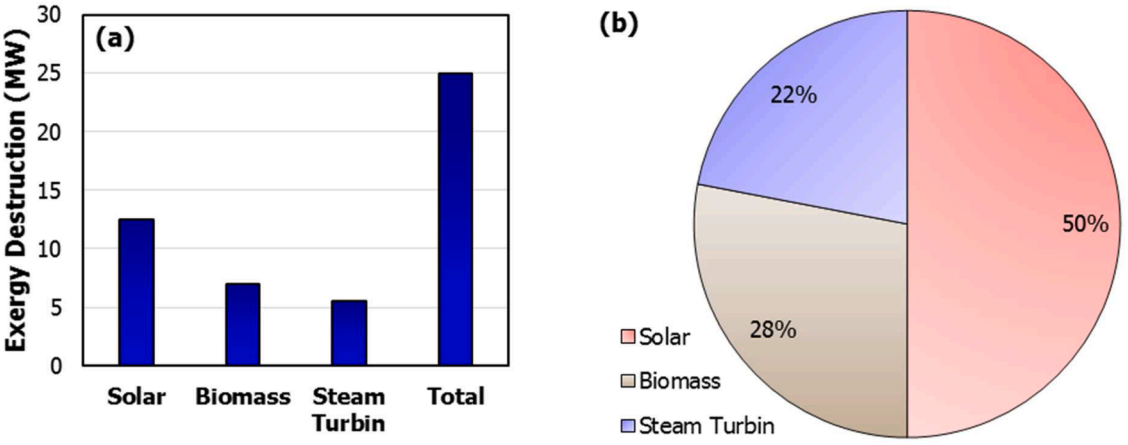

Fig. 4. a) The exergy destruction and b) exergy destruction percentage of the system main components.

Table 4
Comparison of experimental data and numerical modeling results for biomass model.

Production gas component	reference [63]	Current Study
H_2	46.57	43.10
CO	25.84	22.59
CO_2	10.30	9.81
H_2O	17.11	17.05
CH_4	0.090	0.074

the system's parameters.

Heliostat mirrors

After considering technical, practical, and economic factors, the range has been chosen. Within this range, a hybrid system is technically feasible, accounting for engineering challenges and logistical constraints beyond 450 mirrors. Additionally, the range is representative of modern solar power project scale, ensuring relevance to real-world applications. The emphasis on practicality is reflected in our study. The 250–450 range exploration has been prompted by the size of solar fields in existing installations. By examining this range, the hybrid system's behavior at a scale matching industry practices and allowing for future applications is aimed at being revealed. The investigation of the 250–450 heliostat mirror range also sheds light on the hybrid system's scalability. Understanding performance variations and cost implications within the specified range is required when assessing the system's scaling potential for diverse applications.

The changes in exergy efficiency, energy consumption, and total cost are illustrated in Fig. 6, which shows what happens when the number of mirrors is increased from 250 to 450. As the number of mirrors increases, the amount of heat received from the heat source also increases. This leads to an increase in both the production power of the low-pressure gas turbine as well as the exergy destruction of the entire system (Fig. 6a). The total energy yield and the exergy yield of the entire system are depicted in Fig. 6b. This figure demonstrates that the cost of the solar section rises with an increase in the number of mirrors, whereas the cost of the steam turbine section falls with an increase in the number of mirrors. The costliest aspect of the solar section of the system, which accounts for approximately 68 % of the overall cost. The solar field mirrors have the highest cost of any component in the solar industry; as the number of mirrors increases, so does the cost of the entire system (Fig. 6, c and d). Fig. 6d also depicts the effect of the number of mirrors on the destruction of the exergy of the entire system. It demonstrates that as the number of mirrors in the system increases, the amount of exergy that is destroyed by the entire system increases linearly and with a gentle slope.

Inlet steam temperature

A comprehensive examination of the power generation diagram, predicated on the steam turbine's inlet temperature, unveils intricate dynamics deserving in-depth scrutiny. The ascending trend from 450 to 650 °C (Fig. 7a) not only amplifies the power output of the steam turbine but also augments the overall power generated within the cycle. This nuanced interplay underscores the sensitivity of the system to changes in the steam turbine's inlet temperature. Fig. 7b provides a profound insight into this relationship, illustrating a concurrent elevation in both energy yield and exergy as the overall system efficiency improves. The increase in both energy yield and exergy at the same time shows that the system is using its resources more efficiently, which highlights how important it is to have the right temperatures at the inlet of the steam turbine. In the system's normal state, where exergy destruction remains constant at 25 MW, Fig. 7c delves into the economic ramifications. Operating at the highest temperature results in a substantial $175.5 per hour increase in operational costs, while operating at the lowest temperature brings about a noteworthy $173 per hour decrease. This cost sensitivity underscores the economic implications of the steam turbine's operating temperature, introducing a pivotal dimension to the analysis. Fig. 7d encapsulates the holistic changes throughout the system,

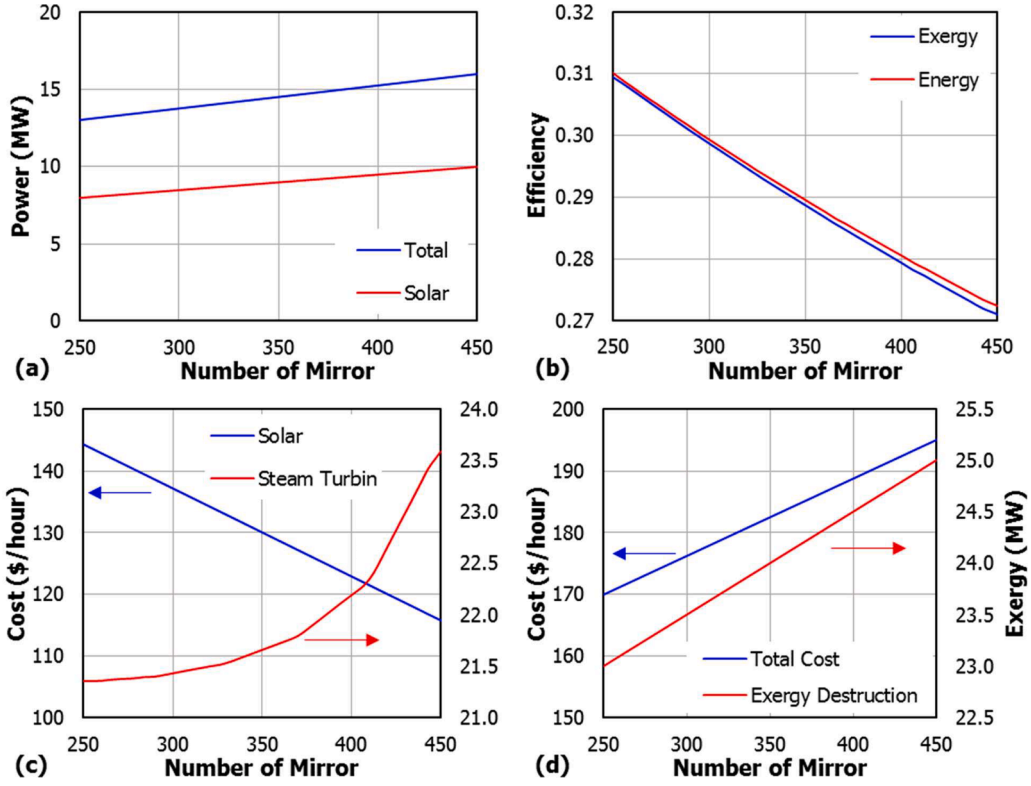

Fig. 6. The Effect of the number of solar heliostats on a) power generation, b) system efficiency, c) solar and steam cost, d) total cost and exergy destruction.

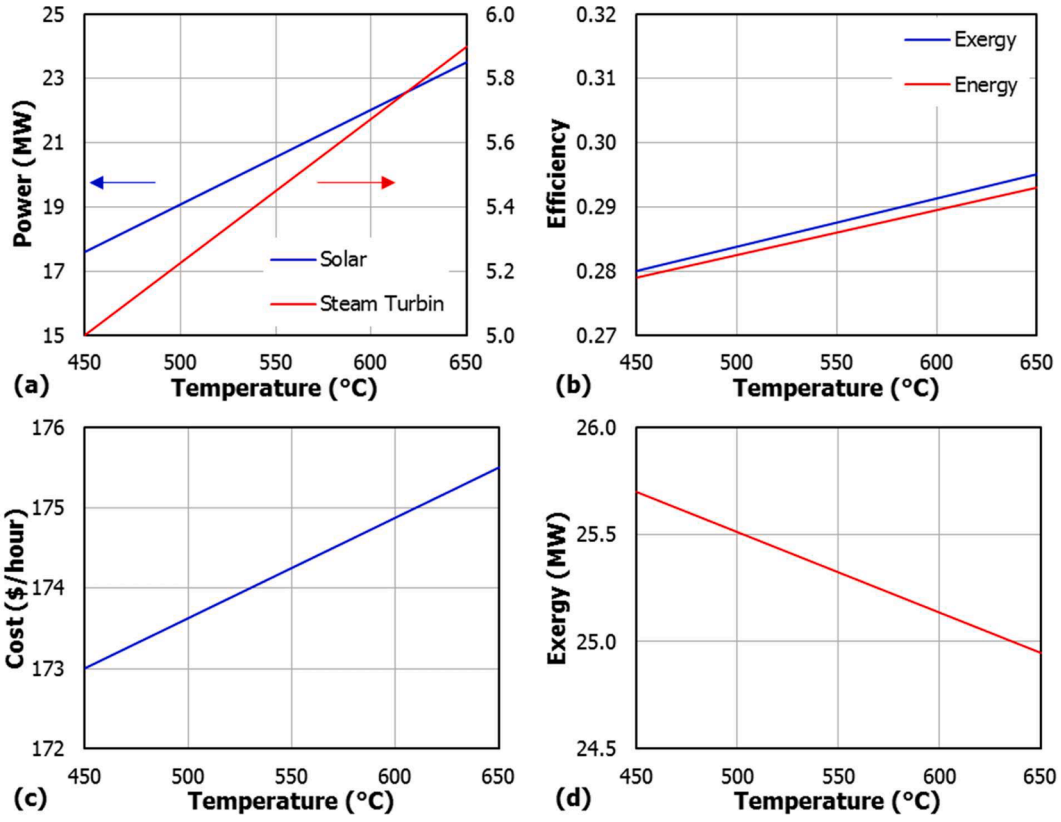

Fig. 7. The Effect of the steam turbine's inlet temperature on a) power generation, b) system efficiency, c) total cost, d) exergy destruction.

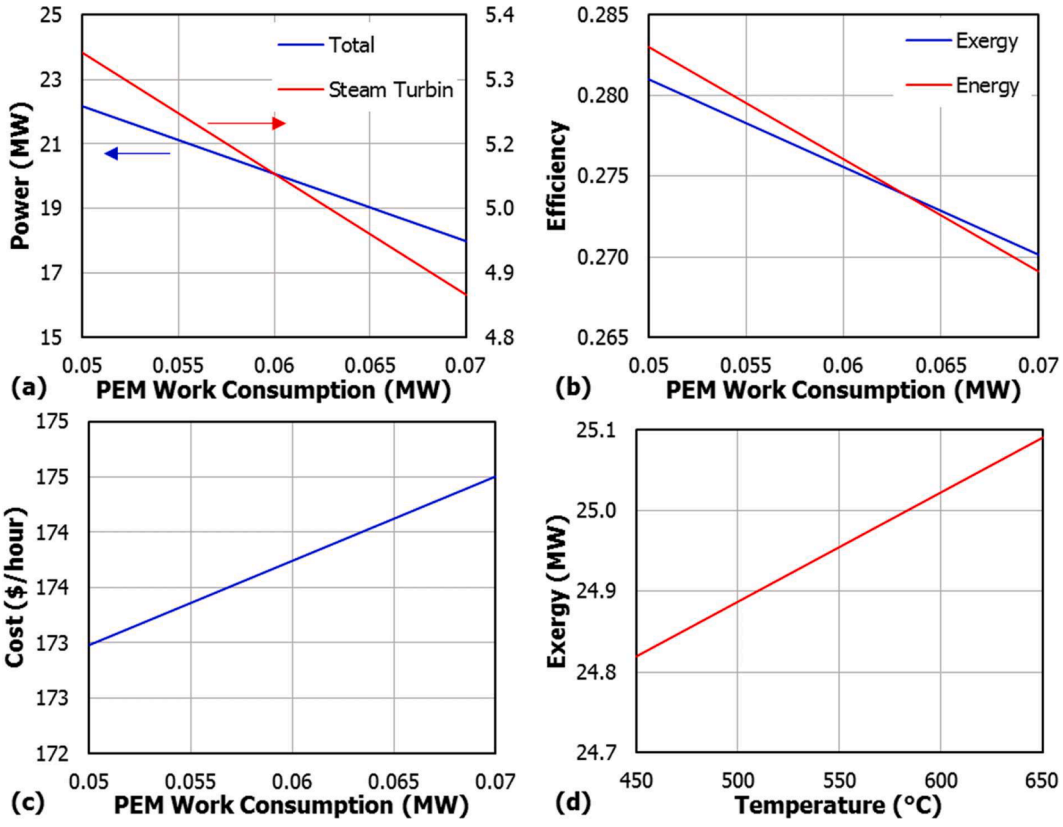

Fig. 8. The Effect of the electrolyzer consumption work on a) power generation, b) system efficiency,.

particularly highlighting the consequential reduction in the exergy destruction rate from 25.71 MW to 24.95 MW when elevating the steam turbine's inlet temperature from 450 to 650 °C. This shift is attributed to an overall decrease in the exergy destruction rate, emphasizing the need for meticulous control over operating temperatures for optimal system performance. The intricate relationship between temperature variations, system efficiency, and operational costs becomes further pronounced, as indicated by the 0.75-MW difference in exergy destruction between the highest and lowest temperatures. This underscores the system's sensitivity to temperature adjustments and the nuanced economic considerations associated with such variations.

Electrolyzer consumption work

In Fig. 8a, the details of how the electrolyzer uses work are shown. It shows a very important relationship: the system's overall power goes down in direct proportion to the electrolyzer's work. This noteworthy correlation signifies that as the electrolyzer's workload intensifies, the power of the entire system diminishes. The downstream effects are graphically depicted in Fig. 8b, showcasing the ensuing reduction in both energy efficiency and exergy of the entire system.

Fig. 8c illuminates a direct and consequential correlation between the power consumption of electrolyzers and the overall cost of the system. Under typical usage conditions, with an operational cost of $178 per hour, the power consumption range of electrolyzers (0.05 to 0.07 MW) precipitates notable total cost fluctuations amounting to $1.52 per hour. This cost sensitivity underscores the economic implications of the electrolyzer's power consumption, presenting a critical facet for consideration in system optimization.

Under heightened resource demands, the system experiences an increase in wasted energy, as graphically depicted. The transition from the system's normal state to the work requiring maximal electrolyzer energy usage results in a loss of 0.27 MW of energy (Fig. 8d). This delineates a crucial point of consideration, emphasizing the trade-off between resource demand and energy efficiency. c) total cost, d) exergy destruction.

Conclusion

The ongoing pursuit of sustainable and efficient energy solutions is pivotal in addressing global energy demand while mitigating environmental impact. In this context, the hybridization of power generation systems has emerged as a promising avenue, offering simultaneous production of power, heat, and hydrogen. This study introduces a novel hybrid power generation system that combines solar and biomass energy sources, subjecting all system components to meticulous analysis from both the first and second thermodynamic perspectives. The solar component and the biomass segment, contributing to heat generation, synergistically yield a remarkable power output of 25 MW—representing the system's maximum solar potential. Exergy destruction assessments pinpoint the solar field as the primary contributor to exergy loss. The subsequent deployment of generated power in a polymer membrane electrolyzer effectively yields hydrogen.

Key findings associated with mirror quantity reveal heightened heat intake and low-pressure gas turbine power production, along with increased overall exergy destruction. The solar section, constituting approximately 68 % of the overall cost, experiences an escalating cost trajectory with an increasing number of mirrors. Temperature variations in the steam turbine section showcase a delicate equilibrium between augmented power generation, heightened system efficiency, and associated operational costs. Elevating the steam turbine's inlet temperature enhances power generation and overall system efficiency, concomitant with a decrease in the exergy destruction rate from 25.71 MW to 24.95 MW. Operating at the highest temperature incurs an increase of $175.5 per hour in the total cost of system operation, while the lowest temperature yields a decrease of $173 per hour. Furthermore, the study elucidates the impact of the electrolyzer's workload on system dynamics. Increasing electrolyzer work correlates with decreased overall system power, resulting in diminished energy efficiency and exergy. Electrolyzer power consumption, within the range of 0.05 to 0.07 MW, precipitates total cost fluctuations of $1.52 per hour. The transition to the energy-intensive work mode causes a notable loss of 0.27 MW of exergy.

This study contributes to a comprehensive understanding of the hybrid system's performance, offering invaluable insights for advancing sustainable energy technologies in the quest for efficient and environmentally conscious power generation.

CRediT authorship contribution statement

Kairat Kuterbekov: Writing – review & editing, Investigation, Funding acquisition, Formal analysis, Data curation. **Asset Kabyshev:** Validation, Software, Resources, Methodology, Conceptualization. **Kenzhebatyr Bekmyrza:** Writing – original draft, Visualization, Validation, Software, Resources, Funding acquisition, Data curation. **Marzhan Kubenova:** Writing – review & editing, Writing – original draft, Methodology, Investigation, Formal analysis.

Declaration of competing interest

The authors declare that they have no known competing financial interests or personal relationships that could have appeared to influence the work reported in this paper.

Data availability

Data will be made available on request.

Acknowledgement

The work was fulfilled in the frame of targeted financing program No. BR21882359, supported by the Ministry of Science and Higher Education of Kazakhstan.

References

[1] N. Hanif, N. Arshed, O. Aziz, On interaction of the energy: human capital Kuznets curve? A case for technology innovation, Environment, Dev. Sustain. 22 (2020) 7559–7586, https://doi.org/10.1007/s10668-019-00536-9.
[2] S. Jasanoff, H.R. Simmet, Renewing the future: excluded imaginaries in the global energy transition, Energy Res. Social Sci. 80 (2021) 102205, https://doi.org/10.1016/j.erss.2021.102205.
[3] S. Opakhai, K. Kuterbekov, Metal-supported solid oxide fuel cells: a review of recent developments and problems, Energies 16 (2023) 4700, https://doi.org/10.3390/en16124700.
[4] H. Azizi, N. Nejatian, Evaluation of the climate change impact on the intensity and return period for drought indices of SPI and SPEI (study area: varamin plain), Water Supply 22 (2022) 4373–4386, https://doi.org/10.2166/ws.2022.056.
[5] H. Eslami, H. Yousefyani, M. Yavary Nia, A. Radice, On how defining and measuring a channel bed elevation impacts key quantities in sediment overloading with supercritical flow, Acta Geophysica 70 (2022) 2511–2528, https://doi.org/10.1007/s11600-022-00851-2.
[6] F. Yavari, S.A. Salehi Neyshabouri, J. Yazdi, A. Molajou, A. Brysiewicz, A novel framework for urban flood damage assessment, Water Resour. Manag. 36 (2022) 1991–2011, https://doi.org/10.1007/s11269-022-03122-3.
[7] F. Shacheri, N.S.R. Nikou, A.N. Ziaei, M. Saeedi, Surface dense discharge from rectangular and trapezoidal channels, Flow Measurement and Instrumentation 87 (2022) 102213, https://doi.org/10.1016/j.flowmeasinst.2022.102213.
[8] O. Adekomaya, T. Majozi, Promoting natural cycle and environmental resilience: a pathway toward sustainable development, South African J. Chem. Eng. 42 (2022) 229–240, https://doi.org/10.1016/j.sajce.2022.09.002.
[9] I. Tajfar, M. Pazoki, A. Pazoki, N. Nejatian, M. Amiri, Analysis of Heating Value of Hydro-Char Produced by Hydrothermal Carbonization of Cigarette Butts, Pollution 9 (2023) 1273–1280, https://doi.org/10.22059/poll.2023.335704.1293.
[10] M.O. Raimi, T.V. Odubo, A.O. Omidiji, Creating the Healthiest Nation: climate Change and Environmental Health Impacts in Nigeria: a Narrative Review, Sustain. Environ. 6 (2021) 61, https://doi.org/10.22158/se.v6n1p61.

[11] O. Shakouri, M.H. Ahmadi, M.F. Gord, Thermodynamic assessment and performance optimization of solid oxide fuel cell-Stirling heat engine–reverse osmosis desalination, Int. J. Low-Carbon Technol. 16 (2021) 417–428, https://doi.org/10.1093/ijlct/ctaa073.
[12] R.R. Peterson, Over the caribbean top: community well-being and over-tourism in small island tourism economies, Int. J. Commun. Well-Being 6 (2023) 89–126, https://doi.org/10.1007/s42413-020-00094-3.
[13] A. Rahman, O. Farrok, M.M. Haque, Environmental impact of renewable energy source based electrical power plants: solar, wind, hydroelectric, biomass, geothermal, tidal, ocean, and osmotic, Renew. Sustain. Energy Rev. 161 (2022) 112279, https://doi.org/10.1016/j.rser.2022.112279.
[14] A.A. Solovyev, A.S. Maznoy, K.A. Kuterbekov, S.A. Nurkenov, S. Opakhai, A. I. Kirdyashkin, V.D. Kitler, N.S. Pichugin, S.V. Rabotkin, I.V. Ionov, Porous Ni–Al–CGO cermet for use in solid oxide fuel cells, Int. J. Self-Propagating High-Temp. Synthesis 28 (2019) 256–261, https://doi.org/10.3103/S1061386219040137.
[15] M.A. Jasim, O.K. Ahmed, Y. Alaiwi, Performance of solar stills integrated with PV/Thermal solar collectors: a review, NTU J. Renew. Energy 4 (2023) 97–111, https://doi.org/10.56286/ntujre.v4i1.456.
[16] A. Giwa, A. Alabi, A. Yusuf, T. Olukan, A comprehensive review on biomass and solar energy for sustainable energy generation in Nigeria, Renew. Sustain. Energy Rev. 69 (2017) 620–641, https://doi.org/10.1016/j.rser.2016.11.160.
[17] A. Aliasghar, P. Javidan, S.A. Rahmaninezhad, N. Mehrdadi, Optimizing the desalination rate in a photoelectrocatalytic desalination cell (PEDC) by altering operational conditions, Water Supply 22 (2022) 8659–8668, https://doi.org/10.2166/ws.2022.379.
[18] A.T. Hoang, S. Nižetić, C.K. Cheng, R. Luque, S. Thomas, T.L. Banh, V.V. Pham, X. P. Nguyen, Heavy metal removal by biomass-derived carbon nanotubes as a greener environmental remediation: a comprehensive review, Chemosphere 287 (2022) 131959, https://doi.org/10.1016/j.chemosphere.2021.131959.
[19] A. Tarafdar, G. Sowmya, K. Yogeshwari, G. Rattu, T. Negi, M.K. Awasthi, A. Hoang, R. Sindhu, R. Sirohi, Environmental pollution mitigation through utilization of carbon dioxide by microalgae, Environ. Pollution 328 (2023) 121623, https://doi.org/10.1016/j.envpol.2023.121623.
[20] Y. Alaiwi, A.M. Abed, G.F. Smaisim, M.A.S. Aly, S.K. Hadrawi, R. Morovati, Simulation and investigation of bioethanol production considering energetic and economic considerations, Int. J. Low-Carbon Technol. 18 (2023) 191–203, https://doi.org/10.1093/ijlct/ctad008.
[21] K. Sivabalan, S. Hassan, H. Ya, J. Pasupuleti, A review on the characteristic of biomass and classification of bioenergy through direct combustion and gasification as an alternative power supply, J. Phy.: Conference Series 1831 (2021) 012033, https://doi.org/10.1088/1742-6596/1831/1/012033.
[22] S. Sharma, S. Agarwal, A. Jain, Significance of hydrogen as economic and environmentally friendly fuel, Energies 14 (2021) 7389, https://doi.org/10.3390/en14217389.
[23] Ö. Tezer, N. Karabağ, A. Öngen, C.Ö. Çolpan, A. Ayol, Biomass gasification for sustainable energy production: a review, Int J Hydrogen Energy 47 (2022) 15419–15433, https://doi.org/10.1016/j.ijhydene.2022.02.158.
[24] M.S. Shahin, M.F. Orhan, K. Saka, A.T. Hamada, F. Uygul, Energy assessment of an integrated hydrogen production system, Int. J. Thermofluids 17 (2023) 100262, https://doi.org/10.1016/j.ijft.2022.100262.
[25] A.G. Olabi, M.A. Abdelkareem, T. Wilberforce, A. Alkhalidi, T. Salameh, A.G. Abo-Khalil, M.M. Hassan, E.T. Sayed, Battery electric vehicles: progress, power electronic converters, strength (S), weakness (W), opportunity (O), and threats (T), Int. J. Thermofluids 16 (2022) 100212, https://doi.org/10.1016/j.ijft.2022.100212.
[26] K. Obaideen, M. Nooman AlMallahi, A.H. Alami, M. Ramadan, M.A. Abdelkareem, N. Shehata, A.G. Olabi, On the contribution of solar energy to sustainable developments goals: case study on Mohammed bin Rashid Al Maktoum Solar Park, Int. J. Thermofluids 12 (2021) 100123, https://doi.org/10.1016/j.ijft.2021.100123.
[27] S.A.H. Naqvi, T. Taner, M. Ozkaymak, H.M. Ali, Hydrogen Production through Alkaline Electrolyzers: a Techno-Economic and Enviro-Economic Analysis, Chem. Eng. Technol. 46 (2023) 474–481, https://doi.org/10.1002/ceat.202200234.
[28] M. Mubarrat, M.M. Mashfy, T. Farhan, M.M. Ehsan, Research advancement and potential prospects of thermal energy storage in concentrated solar power application, Int. J. Thermofluids 20 (2023) 100431, https://doi.org/10.1016/j.ijft.2023.100431.
[29] H. Ishaq, I. Dincer, C. Crawford, A review on hydrogen production and utilization: challenges and opportunities, Int J Hydrogen Energy 47 (2022) 26238–26264, https://doi.org/10.1016/j.ijhydene.2021.11.149.
[30] Z. Stępień, A Comprehensive Overview of Hydrogen-Fueled Internal Combustion Engines: achievements and Future Challenges, Energies 14 (2021) 6504, https://doi.org/10.3390/en14206504.
[31] P.J. Megía, A.J. Vizcaíno, J.A. Calles, A. Carrero, Hydrogen Production Technologies: from Fossil Fuels toward Renewable Sources. A Mini Review, Energy & Fuels 35 (2021) 16403–16415, https://doi.org/10.1021/acs.energyfuels.1c02501.
[32] K. Zeng, D. Zhang, Recent progress in alkaline water electrolysis for hydrogen production and applications, Prog. Energy Combust. Sci. 36 (2010) 307–326, https://doi.org/10.1016/j.pecs.2009.11.002.
[33] K. Scott, Chapter 1. introduction to electrolysis, electrolysers and hydrogen production, RSC Energy and Environ. Series (2019) 1–27, https://doi.org/10.1039/9781788016049-00001.
[34] D. Yu, J. Hu, W. Wang, B. Gu, Comprehensive techno-economic investigation of biomass gasification and nanomaterial based SOFC/SOEC hydrogen production system, Fuel 333 (2023) 126442, https://doi.org/10.1016/j.fuel.2022.126442.
[35] S. Sharafi laleh, M. Zeinali, S.M.S. Mahmoudi, S. Soltani, M.A. Rosen, Biomass co-fired combined cycle with hydrogen production via proton exchange membrane electrolysis and waste heat recovery: thermodynamic assessment, Int J Hydrogen Energy 48 (2023) 33795–33809, https://doi.org/10.1016/j.ijhydene.2023.05.137.
[36] Z. Yang, W. JingChun, Y. Elmasry, A. Alanazi, A. Armghan, M. Alanazi, A. M. Algelany, M. Wae-hayee, Techno-economic and multi objective optimization of zero carbon emission biomass based supercritical carbon dioxide oxy combustion system integrated with carbon dioxide liquefaction system and solid oxide electrolyzer, J. CO2 Utilization 64 (2022) 102169, https://doi.org/10.1016/j.jcou.2022.102169.
[37] Y. Ayub, J. Ren, C. He, C. Azzaro-Pantel, Co-gasification of biomass and plastic waste for green and blue hydrogen Production: novel process development, economic, exergy, advanced exergy, and exergoeconomics analysis, Chem. Eng. J. 480 (2024) 148080, https://doi.org/10.1016/j.cej.2023.148080.
[38] Z. Bai, Q. Liu, J. Lei, X. Wang, J. Sun, H. Jin, Thermodynamic evaluation of a novel solar-biomass hybrid power generation system, Energy Conv. Manag. 142 (2017) 296–306, https://doi.org/10.1016/j.enconman.2017.03.028.
[39] T. Taner, S.A.H. Naqvi, M. Ozkaymak, Techno-economic Analysis of a More Efficient Hydrogen Generation System Prototype: a Case Study of PEM Electrolyzer with Cr-C Coated SS304 Bipolar Plates, Fuel Cells 19 (2019) 19–26, https://doi.org/10.1002/fuce.201700225.
[40] N. Tukenmez, M. Koc, M. Ozturk, A novel combined biomass and solar energy conversion-based multigeneration system with hydrogen and ammonia generation, Int. J. Hydrogen Energy 46 (2021) 16319–16343, https://doi.org/10.1016/j.ijhydene.2021.02.215.
[41] M.E. Burulday, M.S. Mert, N. Javani, Thermodynamic analysis of a parabolic trough solar power plant integrated with a biomass-based hydrogen production system, Int. J. Hydrogen Energy 47 (2022) 19481–19501, https://doi.org/10.1016/j.ijhydene.2022.02.163.
[42] M. Shamsi, A.A. Obaid, S. Farokhi, A. Bayat, A novel process simulation model for hydrogen production via reforming of biomass gasification tar, Int. J. Hydrogen Energy 47 (2022) 772–781, https://doi.org/10.1016/j.ijhydene.2021.10.055.
[43] H. Wang, Z. Su, A.M. Abed, K. Nag, A. Deifalla, M. Marefati, I. Mahariq, Y. Wei, Multi-criteria evaluation and optimization of a new multigeneration cycle based on solid oxide fuel cell and biomass fuel integrated with a thermoelectric generator, gas turbine, and methanation cycle, Process Safety and Environ. Protection 170 (2023) 139–156, https://doi.org/10.1016/j.psep.2022.11.087.
[44] Z. Zakaria, S.K. Kamarudin, A review of alkaline solid polymer membrane in the application of <scp>AEM</scp>electrolyzer: materials and characterization, Int. J. Energy Res. 45 (2021) 18337–18354, https://doi.org/10.1002/er.6983.
[45] S.M. Abu, M.A. Hannan, P.J. Ker, M. Mansor, S.K. Tiong, T.M.I. Mahlia, Recent progress in electrolyser control technologies for hydrogen energy production: a patent landscape analysis and technology updates, J. Energy Storage 72 (2023) 108773, https://doi.org/10.1016/j.est.2023.108773.
[46] S. Singla, N.P. Shetti, S. Basu, K. Mondal, T.M. Aminabhavi, Hydrogen production technologies - Membrane based separation, storage and challenges, J. Environ. Manage. 302 (2022) 113963, https://doi.org/10.1016/j.jenvman.2021.113963.
[47] S. Ding, B. Guo, S. Hu, J. Gu, F. Yang, Y. Li, J. Dang, B. Liu, J. Ma, Analysis of the effect of characteristic parameters and operating conditions on exergy efficiency of alkaline water electrolyzer, J. Power Sour. 537 (2022) 231532, https://doi.org/10.1016/j.jpowsour.2022.231532.
[48] P. Tiam Kapen, B.A. Medjo Nouadje, V. Chegnimonhan, G. Tchuen, R. Tchinda, Techno-economic feasibility of a PV/battery/fuel cell/electrolyzer/biogas hybrid system for energy and hydrogen production in the far north region of cameroon by using HOMER pro, Energy Strategy Rev. 44 (2022) 100988, https://doi.org/10.1016/j.esr.2022.100988.
[49] S. Saeidi, S. Nazari Enjedan, E. Alvandi Behineh, K. Tehranian, S. Jazayerifar, Factors Affecting Public Transportation Use during Pandemic: an Integrated Approach of Technology Acceptance Model and Theory of Planned Behavior, TEHNIČKI GLASNIK /Technical J. (2023), https://doi.org/10.31803/tg-20230601145322.
[50] S. Giddey, S.P.S. Badwal, H. Ju, Polymer Electrolyte Membrane Technologies Integrated With Renewable Energy for Hydrogen Production. Current Trends and Future Developments On (Bio-) Membranes, Elsevier, 2019, pp. 235–259, https://doi.org/10.1016/B978-0-12-813545-7.00010-6.
[51] M. Shaygan, M.A. Ehyaei, A. Ahmadi, M.E.H. Assad, J.L. Silveira, Energy, exergy, advanced exergy and economic analyses of hybrid polymer electrolyte membrane (PEM) fuel cell and photovoltaic cells to produce hydrogen and electricity, J. Clean Prod. 234 (2019) 1082–1093, https://doi.org/10.1016/j.jclepro.2019.06.298.
[52] A.S. Joshi, I. Dincer, B.V. Reddy, Solar hydrogen production: a comparative performance assessment, Int. J. Hydrogen Energy 36 (2011) 11246–11257, https://doi.org/10.1016/j.ijhydene.2010.11.122.
[53] C. BIAKU, N. DALE, M. MANN, H. SALEHFAR, A. PETERS, T. HAN, A semiempirical study of the temperature dependence of the anode charge transfer coefficient of a 6kW PEM electrolyzer, Int. J. Hydrogen Energy 33 (2008) 4247–4254, https://doi.org/10.1016/j.ijhydene.2008.06.006.
[54] R. García-Valverde, N. Espinosa, A. Urbina, Simple PEM water electrolyser model and experimental validation, Int J Hydrogen Energy 37 (2012) 1927–1938, https://doi.org/10.1016/j.ijhydene.2011.09.027.
[55] Z. Abdin, C.J. Webb, E.M. Gray, Modelling and simulation of a proton exchange membrane (PEM) electrolyser cell, Int J Hydrogen Energy 40 (2015) 13243–13257, https://doi.org/10.1016/j.ijhydene.2015.07.129.

[56] F. MARANGIO, M. SANTARELLI, M. CALI, Theoretical model and experimental analysis of a high pressure PEM water electrolyser for hydrogen production, Int. J. Hydrogen Energy 34 (2009) 1143–1158, https://doi.org/10.1016/j.ijhydene.2008.11.083.
[57] A.H. Abdol Rahim, A.S. Tijani, S.K. Kamarudin, S. Hanapi, An overview of polymer electrolyte membrane electrolyzer for hydrogen production: modeling and mass transport, J. Power Sources 309 (2016) 56–65, https://doi.org/10.1016/j.jpowsour.2016.01.012.
[58] R. Rivero, M. Garfias, Standard chemical exergy of elements updated, Energy 31 (2006) 3310–3326, https://doi.org/10.1016/j.energy.2006.03.020.
[59] V.B. Silva, A. Rouboa, Using a two-stage equilibrium model to simulate oxygen air enriched gasification of pine biomass residues, Fuel Proc. Technol. 109 (2013) 111–117, https://doi.org/10.1016/j.fuproc.2012.09.045.
[60] E. Shayan, V. Zare, I. Mirzaee, Hydrogen production from biomass gasification; a theoretical comparison of using different gasification agents, Energy Conv. Manag. 159 (2018) 30–41, https://doi.org/10.1016/j.enconman.2017.12.096.
[61] F. Ranjbar, A. Chitsaz, S.M.S. Mahmoudi, S. Khalilarya, M.A. Rosen, Energy and exergy assessments of a novel trigeneration system based on a solid oxide fuel cell, Energy Conv. Manag. (2014), https://doi.org/10.1016/j.enconman.2014.07.014.
[62] T. Ioroi, K. Yasuda, Z. Siroma, N. Fujiwara, Y. Miyazaki, Thin film electrocatalyst layer for unitized regenerative polymer electrolyte fuel cells, J. Power Sour. 112 (2002) 583–587, https://doi.org/10.1016/S0378-7753(02)00466-4.
[63] G. Schuster, G. Löffler, K. Weigl, H. Hofbauer, Biomass steam gasification – an extensive parametric modeling study, Bioresour. Technol. 77 (2001) 71–79, https://doi.org/10.1016/S0960-8524(00)00115-2.